Structural and Biochemical Characterization of Recombinant Wild Type and a C30A Mutant of Trimethylamine Dehydrogenase from *Methylophilus methylotrophus* (sp. W_3A_1)[†,‡]

Peter Trickey,[§] Jaswir Basran,[||] Lu-Yun Lian,[||,⊥] Zhi-wei Chen,[§] John D. Barton,[§] Michael J. Sutcliffe,[#] Nigel S. Scrutton,[||] and F. Scott Mathews*[,§]

Department of Biochemistry and Molecular Biophysics, Washington University School of Medicine, St. Louis, Missouri 63110, and Departments of Biochemistry and Chemistry and Biological NMR Centre, University of Leicester, Leicester LE1 7RH, U.K.

Received November 29, 1999; Revised Manuscript Received April 14, 2000

ABSTRACT: Trimethylamine dehydrogenase (TMADH) is an iron−sulfur flavoprotein that catalyzes the oxidative demethylation of trimethylamine to form dimethylamine and formaldehyde. It contains a unique flavin, in the form of a 6-*S*-cysteinyl FMN, which is bent by ∼25° along the N5−N10 axis of the flavin isoalloxazine ring. This unusual conformation is thought to modulate the properties of the flavin to facilitate catalysis, and has been postulated to be the result of covalent linkage to Cys-30 at the flavin C6 atom. We report here the crystal structures of recombinant wild-type and the C30A mutant TMADH enzymes, both determined at 2.2 Å resolution. Combined crystallographic and NMR studies reveal the presence of inorganic phosphate in the FMN binding site in the deflavo fraction of both recombinant wild-type and C30A proteins. The presence of tightly bound inorganic phosphate in the recombinant enzymes explains the inability to reconstitute the deflavo forms of the recombinant wild-type and C30A enzymes that are generated in vivo. The active site structure and flavin conformation in C30A TMADH are identical to those in recombinant and native TMADH, thus revealing that, contrary to expectation, the 6-*S*-cysteinyl FMN link is not responsible for the 25° butterfly bending along the N5−N10 axis of the flavin in TMADH. Computational quantum chemistry studies strongly support the proposed role of the butterfly bend in modulating the redox properties of the flavin. Solution studies reveal major differences in the kinetic behavior of the wild-type and C30A proteins. Computational studies reveal a hitherto, unrecognized, contribution made by the S^{γ} atom of Cys-30 to substrate binding, and a role for Cys-30 in the optimal geometrical alignment of substrate with the 6-*S*-cysteinyl FMN in the enzyme active site.

Trimethylamine dehydrogenase (TMADH; EC 1.5.99.7)[1] is an iron−sulfur flavoprotein from *Methylophilus methylotrophus* (sp. W_3A_1) that catalyzes the oxidative N-demethylation of trimethylamine by water with formation of dimethylamine and formaldehyde (*1*):

$$(CH_3)_3N + H_2O \rightarrow (CH_3)_2NH + CH_2O + 2H^+ + 2e^-$$

The enzyme is a homodimer of molecular mass 166 kDa. Each subunit contains one [4Fe-4S] center and one molecule each of FMN and ADP [Figure 1A; (*2*)]. The FMN is bound covalently through the C6 position of the flavin isoalloxazine ring to a cysteine side chain at position 30 of the molecule (*3*−*6*). The binding site for FMN is at the C-terminal end of a parallel $\beta_8\alpha_8$ TIM barrel (*2*), in a similar position to the FMN in flavocytochrome b_2 (*7*) and old yellow enzyme (*8*). An unusual feature of TMADH, however, is the high degree of butterfly bending of the 6-*S*-cysteinyl FMN in the oxidized enzyme (Figure 1B). It has been suggested that the flavin conformation may exert fine control on the flavin reduction potential (*9*). The possibility exists with TMADH that butterfly bending of the flavin may be a consequence of tethering the isoalloxazine ring to the protein via the thioether bond of the 6-*S*-cysteinyl FMN.

TMADH has been cloned and sequenced (*10*); the structure of the wild-type enzyme was determined at 2.4 Å resolution (*2*) and reported on the basis of a partial amino acid sequence (*11*),[2] and the refinement has been extended to 1.7 Å resolution (Mathews et al., unpublished). The wild-type enzyme can be expressed in *E. coli* at high levels (*10*, *12*)

[†] This work has been supported in part by USPHS Grant GM31611 (F.S.M.) and by grants from the UK Biotechnology and Biological Sciences Research Council and the Lister Insititute for Preventive Medicine (N.S.S. and M.J.S.). N.S.S. is a Lister Institute Research Professor.

[‡] Crystallographic coordinates have been deposited in the Protein Data Bank under file names 1DJN and 1DJQ.

* Correspondence should be addressed to this author at the Department of Biochemistry and Molecular Biophysics, Washington University School of Medicine, St. Louis, MO 63110. Tel: 314 362 1080; FAX: 314 362 7183; E-mail: mathews@biochem.wustl.edu.

[§] Department of Biochemistry and Molecular Biophysics, Washington University School of Medicine.

[||] Department of Biochemistry, University of Leicester.

[⊥] Biological NMR Centre, University of Leicester.

[#] Department of Chemistry, University of Leicester.

[1] Abbreviations: TMADH, trimethylamine dehydrogenase; 2,4-DNP, 2,4-dinitrophenylhydrazine; rms, root-mean-square.

[2] Coordinates at 2.4 Å resolution based on the gene sequence of TMADH (*10*) are deposited with the Protein Data Bank, accession code 2TMD.

10.1021/bi9927181 CCC: $19.00
Published on Web 06/08/2000

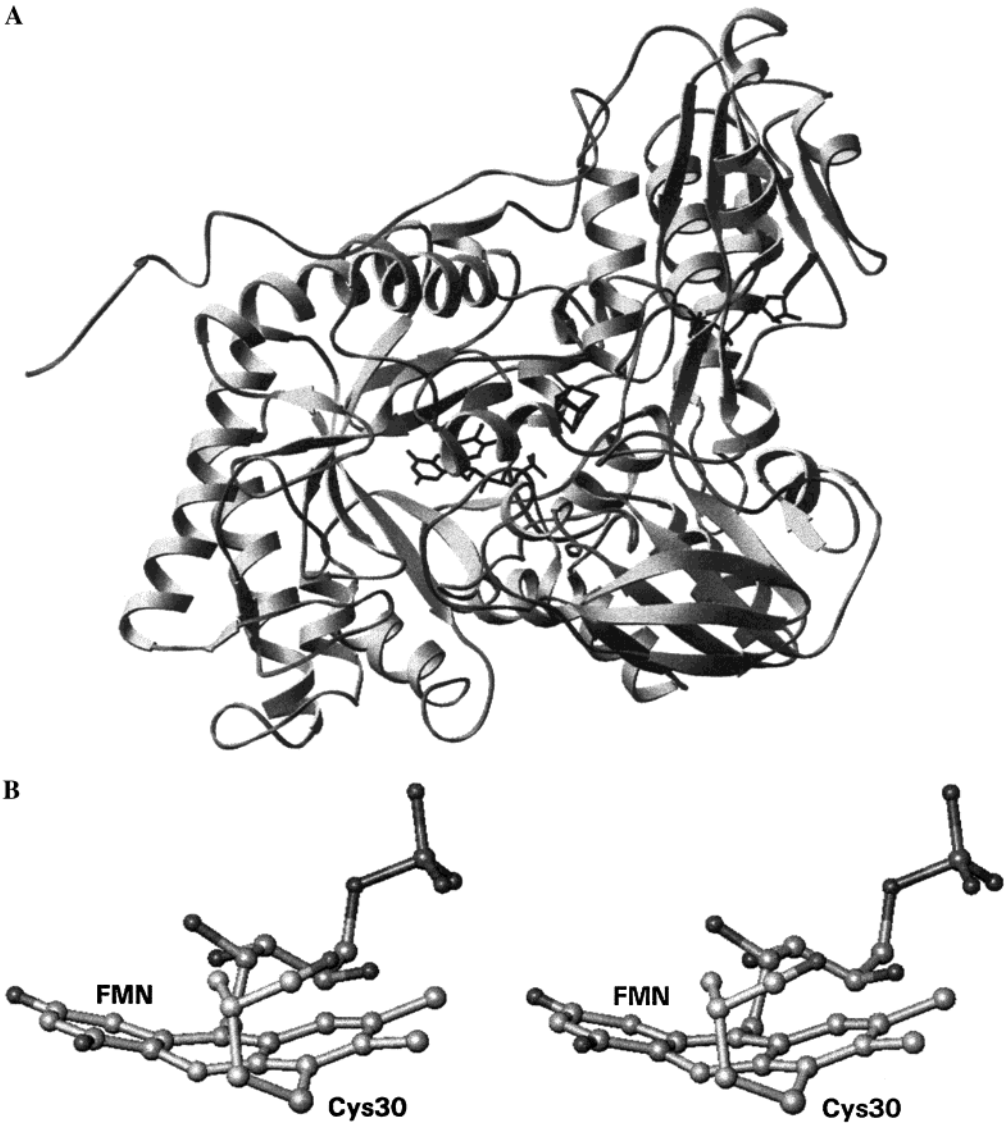

FIGURE 1: Structure of native TMADH. (A) Ribbon diagram of TMADH. The FMN, ADP, and iron−sulfur center are black stick figures. This diagram was generated using RIBBONS (*40*). (B) Stereo diagram of FMN and the ligand, Cys-30, covalently attached to the C6 position of FMN. This diagram was generated using Turbo-Frodo (*19*).

and binds stoichiometric amounts of ADP and fully intact iron−sulfur centers noncovalently, but binds only substoichiometric amounts of FMN covalently, at the level of 30−50% (*12*). The remainder of the enzyme is incapable of binding additional flavin. However, the flavinylated fraction is fully active and behaves the same as the wild-type enzyme under steady-state and stopped-flow conditions (*12*, *13*). A mutant of TMADH has been prepared and characterized in which Cys-30 has been replaced by Ala. The mutant is active in the demethylation of trimethylamine (*12*), but steady-state turnover leads to progressive inactivation of the enzyme due to the formation of 6-hydroxy FMN (*13*). A mechanism for inactivation has been proposed involving the flavin iminoquinone methide tautomer of FMN (*14*). Formation of the tautomer is thought to enhance the electrophilicity of the C6 atom of the flavin. The covalent link between Cys-30 and the C6 atom of the flavin thus prevents hydroxylation of the flavin at the C6 position in the wild-type enzyme.

Like the recombinant wild-type enzyme, the C30A mutant also binds FMN at a diminished level, as well as a full complement of the iron−sulfur center and ADP (*12*). Removal of the flavin from the C30A mutant using chaotropic agents is reversible, and reconstitution with FMN restores full activity, but only up to the original level of flavinylation (*12*). Single-turnover stopped-flow studies with the nonphysiological slow substrate diethylmethylamine (DEMA) have demonstrated that the C30A mutant TMADH has approximately one-sixth the flavin reduction rate of wild-type enzyme, although the dissociation constant for substrate and other steps in the reductive half-reaction are essentially unaffected (*13*).

In this paper, we present an analysis of the structural and biochemical properties of recombinant TMADH and the C30A mutant of the enzyme. The methods used for this characterization include X-ray crystallography, stopped-flow kinetic measurements, ^{31}P NMR, and computational chemistry. We demonstrate that the structure of the C30A mutant is essentially identical to that of recombinant wild-type, thus revealing that the 6-*S*-cysteinyl FMN does not facilitate butterfly bending of the flavin isoalloxazine ring. Combined crystallographic and NMR studies have been used to demonstrate the presence of inorganic phosphate in the 5′-phosphate binding site for FMN, thus explaining why reconstitution of the deflavo protein with FMN is not

Table 1: Data Collection and Refinement Statistics for Recombinant Wild-Type and C30A Mutant TMADH Enzymes

	recombinant TMADH	C30A TMADH mutant
data collection		
resolution (all/outer) (Å)	50.0−2.22/ 2.32−2.22	50.0−2.22/ 2.32−2.22
no. of reflections	81423	81611
completeness (all/outer) (%)	93.8/70.9	93.4/71.7
R_{merge} (all/outer) (%)[a]	5.2/13.2	5.5/12.3
$\langle I/\sigma(I)\rangle$ (all/outer)[b]	17.0/4.4	22.2/6.4
redundancy (all/outer)	3.2/2.2	4.0/2.4
refinement		
resolution (Å)	8.0−2.2	8.0−2.2
R[c]	13.9	13.9
R_{free}[c,d]	18.5	18.7
no. of protein atoms (non-H)	11614	11612
$\langle B\rangle$ (main chain atoms) (Å^2)	21.3	20.8
$\langle B\rangle$ (side chain atoms) (Å^2)	19.5	23.4
rms ΔB (main chain−main chain) (Å^2)	2.1	1.9
rms ΔB (side chain−side chain) (Å^2)	3.6	3.3
no. of solvent molecules	653	661
$\langle B\rangle$ (Å^2)	28.7	28.5
rms deviation, bond lengths (Å)	0.008	0.008
rms deviation, bond angles (deg)	1.40	1.56

[a] $R_{merge} = \Sigma_h\Sigma_i|I(h) - I_i(h)|/\Sigma_h\Sigma_i I_i(h)$, where $I_i(h)$ and $I(h)$ are the ith and mean measurement of reflection h, respectively. [b] $I/\sigma(I)$ is the average signal-to-noise ratio for merged reflection intensities. [c] $R = \Sigma_h|F_o - F_c|/\Sigma_h F_o$, where F_o and F_c are the observed and calculated structure factor amplitudes, respectively, of reflection h. [d] R_{free} is the test reflection data set, about 10% selected randomly for cross-validation during crystallographic refinement (*37*).

possible. Additionally, stopped-flow kinetic and computational methods are used to demonstrate and rationalize the different kinetic behaviors of the C30A and wild-type proteins observed with the physiological substrate trimethylamine.

EXPERIMENTAL PROCEDURES

X-ray Crystallography. The recombinant wild-type and C30A mutant proteins were prepared as described previously (*13*). Crystals of both enzyme forms were grown by macroseeding, starting with microcrystals prepared from the native wild-type enzyme by the hanging drop method or by crushing a single crystal (*2*). At least two rounds of seeding were carried out in both cases to ensure thorough dilution of the original seeds. Data from each recombinant form were recorded at room temperature on a Xuong-Hamlin area detector to 2.2 Å resolution using a Rigaku RU200 rotating anode X-ray source, as described previously (*2*). The crystals were isomorphous with the native wild-type enzyme, space group $P2_1$ with unit cell parameters $a = 148.1$ Å, $b = 72.0$ Å, $c = 83.8$ Å, and $\beta = 97.7°$, and contained one homodimer of TMADH in the asymmetric unit. The data were reduced and scaled using software developed at the University of California, San Diego (*15*). The data collection statistics are presented in Table 1.

The recombinant native and C30A structure factors were each locally scaled to the 1.7 Å native TMADH data (Mathews et al., unpublished results) using the ROCKS program package (*16*) as implemented for the VAX computer (*17*). Isomorphous difference electron density maps were computed using Fourier coefficients: $[F_R(h) - F_N(h)]\exp[-i\alpha_N(h)]$ where $F_N(h)$ and $F_R(h)$ are the native and recombinant wild-type or C30A mutant structure factor amplitudes and $\alpha_N(h)$ is the native protein phase angle, calculated from the 1.7 Å model of TMADH.

Refinement of the native and C30A structures was carried out using X-PLOR (*18*) on a Silicon Graphics (SGI) Challenge computer; model building was carried out using Turbo-Frodo (*19*) on an SGI graphics workstation. Weak noncrystallographic symmetry (NCS) restraints were introduced into the refinement (with NCS weights = 20), and the differences between *B*-factors for bonded atoms were restrained (target standard deviations of 2 Å^2 for main chain atoms and 2.5 Å^2 for side chain atoms).

NMR Methods. ^{31}P NMR spectra were recorded at 30 °C using a Bruker AMX600 spectrometer at 242.94 MHz in a 5 mm inverse probe head. All NMR spectra were acquired using a 90° pulse width of 12 μs, with broad-band proton decoupling, and with pulse intervals of 1.5 s. The chemical shifts were referenced to trimethyl phosphate at 0 ppm. The data were processed with a Gaussian window function and using a line-broadening of 40 Hz. For the ^{31}P NMR experiment, the protein was prepared by first dialyzing exhaustively against 20 mM diethylmalonic acid, pH 7.5, in order to remove free phosphate ions from the sample. The final NMR sample was dissolved in 20 mM diethylmalonic acid, in D_2O, pH 7.5, at a final concentration of 1 mM.

Kinetic Methods. Rapid kinetic experiments were performed using an Applied Photophysics SX.18MV stopped-flow spectrophotometer as described previously for the wild-type (*20*) and C30A enzymes (*13*). Absorbance changes were analyzed using nonlinear least-squares regression on an Archimedes 410-1 microcomputer using Spectrakinetics software (Applied Photophysics). Experiments were performed by mixing TMADH in buffer of the desired pH with an equal volume of trimethylamine at the desired concentration in the same buffer. The concentration of substrate was always at least 10-fold greater than that of TMADH, thereby ensuring pseudo-first-order conditions. For each substrate concentration used, at least four replicate measurements were collected and averaged. Substrate-reduced TMADH is quite stable to reoxidation in aerobic environments [half-life about 50 min; (*21*)], and consequently these stopped-flow experiments were carried out under aerobic conditions. The observed rate constants for flavin reduction for the C30A TMADH were found to exhibit hyperbolic dependence on substrate concentration, and the reaction sequence was modeled as shown in the general scheme:

$$\mathrm{TMADH_{ox}} + \mathrm{TMA} \overset{K_d}{\rightleftharpoons} \mathrm{TMADH_{ox}{\cdot}TMA} \xrightarrow{k_{red}} \mathrm{TMADH_{red}} + \mathrm{P} \quad (1)$$

Data were then fitted to obtain K_d and k_{red} values using $k_{obs} = k_{red}[S]/(K_d + [S])$ (*22*). This simplified equation assumes an irreversible chemical step and is justified, since the fit to experimental data passes through the origin. As noted previously for the wild-type TMADH at pH 7.5, the concentration dependence of the reaction rate deviates

slightly from a simple hyperbolic expression (*23*). The chemical step for wild-type TMADH is irreversible, and the condition $k_1[S] + k_2 \gg k_{red}$ is not met [where $K_d = k_2/k_1$ (*23*)]. For native TMADH, the equation derived by Hiromi was therefore used in data fitting (*24*), but in the simplifying limit where electron transfer to native TMADH is irreversible.

Computational Methods. To aid in the interpretation of the kinetic results, computational chemistry studies were carried out on two different flavins—lumiflavin (a model system for the flavin present in the C30A TMADH) and C6-methylsulfanyllumiflavin (a model system for the flavin in wild-type TMADH)—using the software package PC Spartan Plus (Wave function Inc., Irvine, CA). Geometry optimizations, followed by ab initio calculations, were performed using the Hartree−Fock self-consistent field method with the 3-21G* basis set. To investigate the role in modulation of reduction potential by the butterfly bend in the flavin, two sets of calculations were performed—one with all the atoms in the lumiflavin and C6-methylsulfanyllumiflavin free to move (i.e., no atom positions were fixed), and one with all the non-hydrogen atoms fixed to their positions in the crystallographically determined butterfly bent conformation. Electrostatic isopotential surfaces were then calculated, the electrostatic potential was mapped to the molecular surface, and the energy of the lowest unoccupied molecular orbital (LUMO) was calculated. Two-electron reduction potentials were calculated from the energy of the LUMO using the relationship (*25*):[3]

$$[\text{two-electron reduction potential (mV)}] = -241 \times [\text{LUMO energy (eV)}] - 60 \quad (2)$$

RESULTS AND DISCUSSION

X-ray Crystallography: Difference Electron Density Maps. For both the recombinant wild-type and the C30A mutant crystals, almost all of the significant isomorphous difference electron density, for which $|\rho| > 4\sigma(\rho)$ [where ρ is the electron density and $\sigma(\rho)$ is the standard deviation of ρ and is approximated by the root-mean-square (rms) electron density], is located in two slab-shaped volumes, approximately $20 \times 15 \times 10$ Å^3 in size, and located near the center of the FMN positions. Elsewhere the maps are essentially featureless.

The isomorphous difference map between the recombinant and wild-type TMADH shows a region of strong negative electron density surrounding the FMN in both subunits (Figure 2A). This negative density can be explained by the low level of flavin incorporation, estimated to be about 40% from the visible absorption spectrum as compared to the wild-type enzyme (*12*). One important feature of the difference density is that it does not envelop the phosphate group of FMN. This suggests that the phosphate binding sites are fully occupied in the recombinant enzyme, either by the phosphate of FMN or by inorganic phosphate or other similar anions present in the *E. coli* cells during protein synthesis. The most negative point of the difference density [$-21\ \sigma(\rho)$] coincides with the sulfur atom of cysteine-30, the covalent ligand to the C6 position of the flavin ring. There is a positive peak [$10\ \sigma(\rho)$], not shown near the Cys-30 C^β atom, which is related to the negative peak by a rotation of about 105° about the $C^\alpha-C^\beta$ bond, and probably represents an alternate site for the sulfur atom, indicating that Cys-30 is partially disordered in the nonflavinylated portion of the enzyme.

The isomorphous difference electron density for the C30A mutant is very similar to that of the recombinant enzyme (Figure 2B). In particular, the magnitude of the density over the flavin ring and ribityl chain is roughly the same as that in the recombinant protein, indicating approximately the same level of flavinylation. At the phosphate site, the difference density is also low in magnitude, again suggesting full occupation of this site, either by inorganic phosphate or by a similar anion. The negative electron density [at $-37\ \sigma(\rho)$] at the site of the C30 sulfur atom of the wild-type protein is greater in magnitude than in the recombinant enzyme, by nearly a factor of 2. The increased magnitude of the difference density at the sulfur site reflects the replacement of this residue by alanine.

Qualitative evaluation of the two difference maps shows that significant negative difference electron density largely surrounds the riboflavin moiety, or is associated with a few side chains such as Arg-222, Met-362, and Trp355 (in addition to Cys-30 S^γ mentioned above), all in the active site, plus a few isolated peaks. The positive difference electron density consists mostly of discrete spheres that are isolated from the polypeptide chain and are adjacent to the FMN moiety. These positive peaks could represent water molecules present in the deflavo fraction of the protein that occupy space near the vacated volume of the FMN. In a few instances (for example, near Trp-355), there is paired positive and negative density that might indicate slight movement of the side chain with respect to the native wild-type enzyme.

Structure Refinement. Since crystals of both recombinant forms of TMADH were isomorphous with the native, their structures were refined directly, starting from the coordinates for the native structure, but with solvent molecules and the S^γ atom of Cys-30 omitted. After 100 cycles of positional and 30 cycles of temperature factor refinement, the conventional *R*-factors (and R_{Free}) were 0.192 (0.249) and 0.193 (0.255), respectively, for the recombinant and C30A mutant crystals. Further refinement using simulated annealing, followed by interactive model building and solvent placement, was carried out using electron density maps calculated with Fourier coefficients $2F_o - F_c$, where F_o and F_c are the observed and calculated structure factors, respectively.

The refined models of the wild-type recombinant and C30A TMADH structures have excellent geometry (Table 1). The Ramachandran plots indicate that 99.9% of the non-glycine and non-proline residues of the recombinant and 100% of these residues for the C30A mutant are in the most favored and additionally allowed regions (*26*) and none are in disallowed regions of conformational space. The final *R* values (and R_{Free}) are 0.137 (0.183) for the recombinant and 0.137 (0.184) for the C30A structures. Electron density maps based on $2F_o - F_c$ coefficients for the recombinant and C30A mutants in the region containing FMN are shown in Figure

[3] It has been shown that there is good correlation between the experimentally measured two-electron reduction potential and the calculated LUMO energy in flavins for a variety of substituents at the C8 position (*25*). This enabled the linear relationship in eq 2 to be derived (*25*); eq 2 is specific to the 3-21G* basis set.

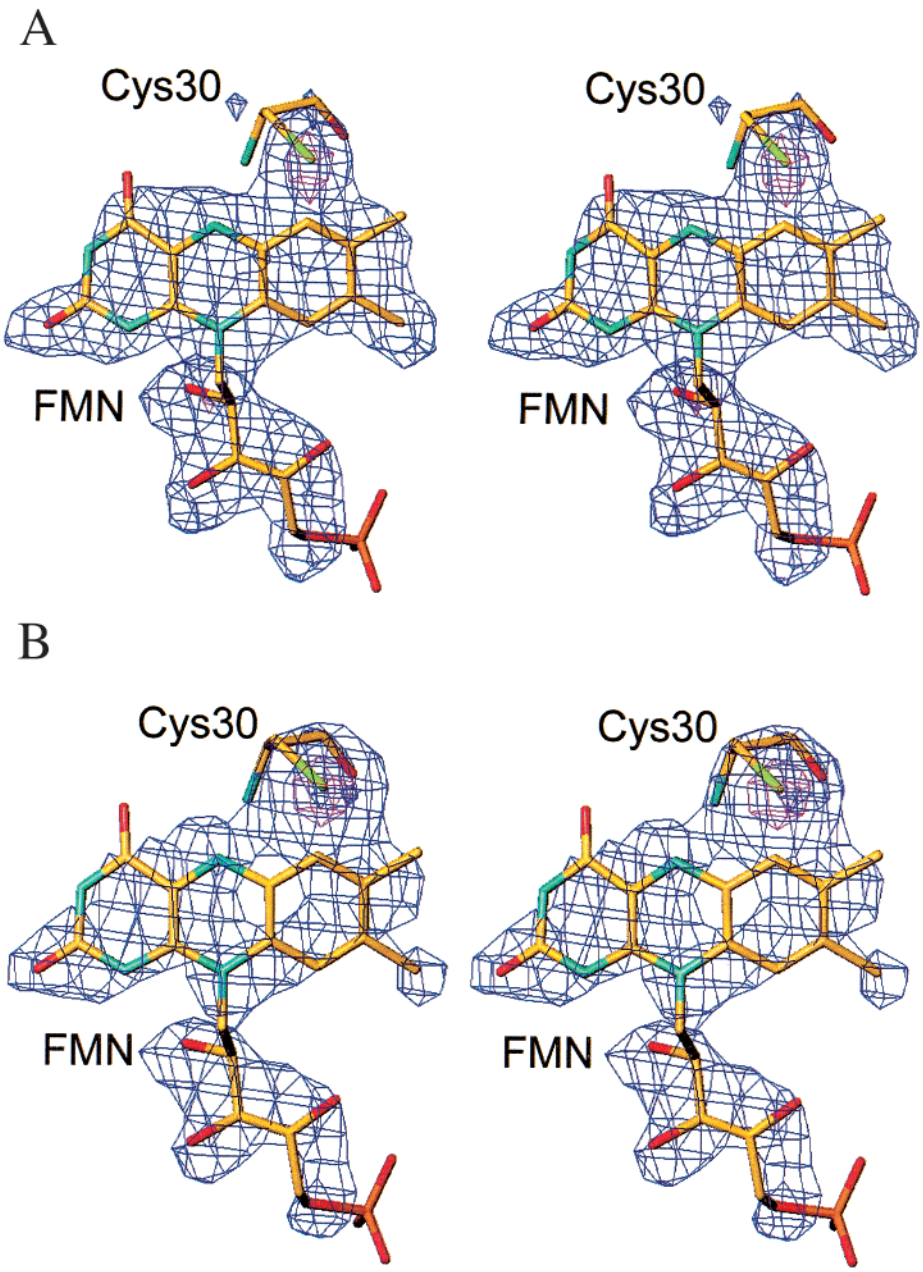

FIGURE 2: Stereoscopic view of isomorphous difference electron density maps. (A) Recombinant minus native wild type. Blue contours are drawn at $-5\ \sigma$ and red contours at $-15\ \sigma$. (B) C30A mutant minus native TMADH isomorphous difference map. Blue contours are drawn at $-5\ \sigma$ and red contours at $-25\ \sigma$. This diagram was generated using Turbo-Frodo (*19*).

3A and Figure 3B, respectively. The refinement statistics are presented in Table 1.

After initial refinement of the two structures, the average *B*-factors for the riboflavin moiety of FMN in both subunits differed from those of the ribityl phosphate groups (Table 2). In contrast, in both subunits of the native wild-type enzyme the average *B*-factors for the riboflavin and phosphate groups of FMN are nearly the same. In all cases, the thermal parameters for subunit 2 are somewhat higher than those for subunit 1. This disparity in temperature factors suggested that the riboflavin portions of FMN are only partially occupied, which is consistent with the interpretation of the isomorphous electron density difference maps. To obtain a quantitative estimate of this occupancy, the temperature factors of the FMN atoms in both structures were set to the average FMN *B*-factors in the native 1.7 Å resolution structure, and the occupancies of the riboflavin moieties were refined. Positional and temperature factor refinement was then repeated, and the occupancies were again refined. The average FMN occupancies are 0.55 for the recombinant wild type and 0.60 for the C30A mutant. These values differ from estimates of the FMN content of 35% for the wild-type recombinant enzyme and of 20% for the C30A enzyme based on solution spectra of the proteins recorded prior to crystallization. The differences between the estimations of flavin content based on the spectra and the refined occupancy may result from some selectivity for the flavinylated enzyme during crystallization.

Except for the decreased flavin content and the disorder or absence of the C30 side chain, both of the recombinant

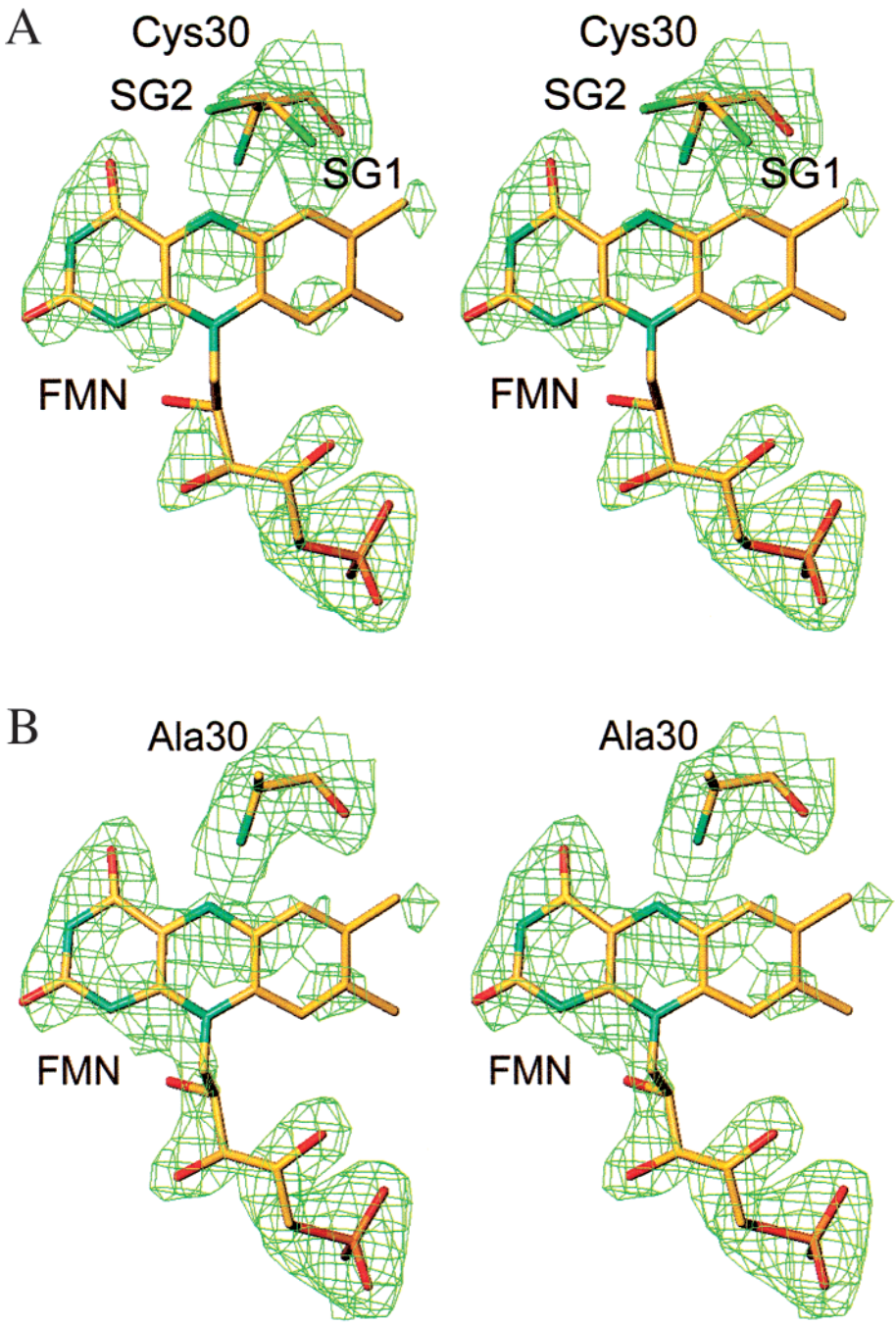

FIGURE 3: $2F_o - F_c$ electron density maps of TMADH in the vicinity of the FMN. Contours are drawn in green at 1 σ. (A) Recombinant native enzyme. The labels SG1 and SG2 refer to the sulfur positions of the two alternate conformers of Cys-30. (B) C30A mutant enzyme. This diagram was generated using Turbo-Frodo (*19*).

Table 2: Average Refined Temperature Factors (Å^2)[a] of Riboflavin and Phosphate Components of FMN in Native and Recombinant TMADH

	subunit 1		subunit 2	
	phosphate	riboflavin	phosphate	riboflavin
native	13.2	13.2	18.5	17.1
recomb	12.2	24.9	18.6	25.9
C30A	14.3	24.0	19.6	26.5

[a] The differences between temperature factors for the bonded atoms of FMN were restrained as described under Experimental Procedures.

structures are very similar to the native. The root-mean-square difference in C_α position is 0.12 Å. Both recombinant structures consist of a random mixture of flavo and deflavo enzyme. Thus, the refined structures will represent an average of these structures.

^{31}P NMR Studies and Flavinylation of TMADH. The ^{31}P NMR spectrum of native, nonrecombinant TMADH shows three peaks centered around 4.25, 1.0, and −11.13 ppm, corresponding respectively to the ^{31}P resonance from FMN, inorganic phosphate, and ADP (Figure 4). The inorganic phosphate peak comes from the remnant phosphate ion in the buffer. The integrated areas under the FMN and ADP resonances suggest that the FMN and ADP contents in the protein are approximately equal, consistent with the known properties of the native enzyme. Recombinant TMADH

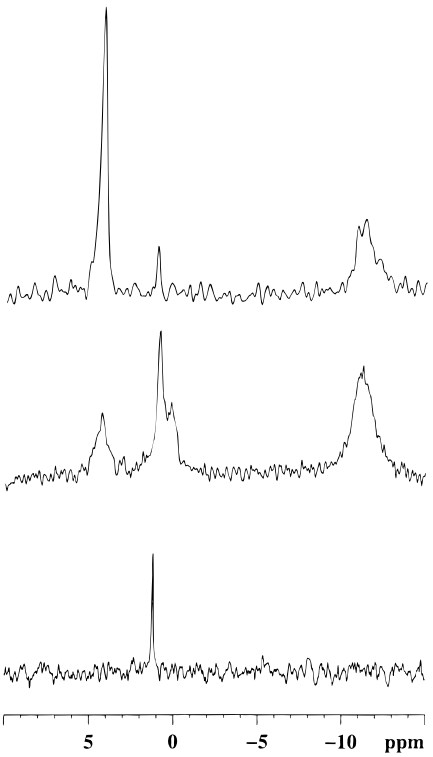

FIGURE 4: ^{31}P NMR spectra of native nonrecombinant TMADH and native recombinant TMADH. Upper spectrum, native nonrecombinant TMADH; middle spectrum, native recombinant TMADH; lower spectrum, buffer spiked with inorganic phosphate. The three peaks centered around 4.25, 1.0, and −11.13 ppm correspond respectively to the ^{31}P resonance from FMN, inorganic phosphate, and ADP. The 1.0 ppm peak is assigned to residual unbound inorganic phosphate, and the shoulder is assigned to enzyme-bound phosphate.

produced a similar spectrum to the native protein, but with two exceptions: there is an extra resonance at 0.14 ppm, and the integrated area of the FMN signal is lower than that of the ADP signal. Since all the NMR spectra were acquired under identical conditions, it can be concluded that the difference in the intensity reflects a lower content of FMN in the recombinant protein, as shown by our previous results (*12*). The extra signal at 0.14 ppm is attributed to the bound inorganic phosphate group, thus confirming that phosphate (and thus not, for example, sulfate) is the anion in the ribityl 5-phosphate binding site observed in the difference electron density maps described above. The bound inorganic phosphate and FMN signals in recombinant wild-type TMADH do not sum to full occupancy. The data, therefore, cannot rule out the possible presence of small amounts of other inorganic anions (e.g., sulfate) in the 5′-phosphate binding site.

Covalent attachment of the flavin to the wild-type enzyme is thought to be a self-catalytic event (*12*). The limitation of the flavinylation of TMADH during overexpression in *E. coli* was previously attributed to the inability of the organism to deliver FMN at the site of protein synthesis rapidly enough to keep up with the production of the enzyme. The inability of the nonflavinylated products to add flavin in vitro was believed to result from some type of misfolding, which could not be reversed even by mild chaotropic agents such as potassium bromide. The NMR results show that the binding site for the ribityl phosphate of FMN is occupied by an inorganic phosphate anion. Once bound, a phosphate ion could be very difficult to remove because of its high affinity for the site and the overall structural stability of TMADH. Indeed, attempts have been made to remove the bound inorganic phosphate anion from the ribityl phosphate binding site. Various methods were tried, including (i) the use of chaotropic agents such as potassium bromide, (ii) incubation in the presence of calcium chloride, and (iii) more aggressive procedures employing urea and guanidine hydrochloride; all of these were without success. These observations thus indicate that the inorganic phosphate anion is bound tightly, as also suggested by the NMR data. Attempted reconstitution of the deflavo fraction of TMADH (containing the inorganic phosphate anion in the 5′-ribityl phosphate binding site) with riboflavin was also unsuccessful.

The high affinity of the phosphate binding site may arise from the numerous ionic and hydrogen bonding interactions and the presence of a helix dipole near the ribityl phosphate oriented with its positive end directed at the negatively charged group [(*2*); Mathews et al., unpublished results]. The stable folding of the TMADH molecule is evidenced by its retention of secondary or tertiary structure even in the presence of SDS (*27*). The fact that only the fraction of the deflavinylated C30A mutant that originally contained flavin is capable of rebinding free FMN (*12*) indicated that two noninterconvertible forms of deflavo TMADH can coexist. The fraction thought to be "misfolded" now appears to be locked into a form in which the bound phosphate anion cannot easily be replaced by FMN. Conversely, the reversibility of FMN removal from the flavinylated portion of the C30A mutant indicates that residual inorganic phosphate is unable to bind to the deflavinyated fraction of the enzyme, although FMN can bind. This suggests that there may still remain some subtle structural difference between the two enzyme forms. It may be possible in the future to find appropriate partially denaturing conditions which will allow phosphate to dissociate from the apoenzyme, yet will not irreversibly disrupt the iron−sulfur cluster or the ADP binding site. This might then lead to development of methods to obtain full incorporation of FMN into recombinant TMADH, facilitating complete structure analysis of a variety of TMADH mutants.

Kinetic Studies of Flavin Reduction and Inactivation. The reactions of wild-type TMADH and the C30A mutant have been investigated previously with the slow substrate diethylmethylamine (*13*). These studies revealed that the limiting rate of flavin reduction was approximately 6-fold less with the C30A mutant (80 s^{-1}) compared with wild type (480 s^{-1}) at pH 7.5. The rate of internal electron transfer to the 4Fe-4S center of TMADH and the rate of formation of the so-called spin-interacting state were unaffected by the mutation. No increase in the substrate dissociation constant was observed with DEMA following mutation. However, it is important to emphasize that DEMA is a slow, nonphysiological substrate that binds with low affinity ($K_d \sim 5$ mM) to wild-type TMADH (*13*). Data for the reactions of wild-type and C30A TMADH enzymes with the physiological substrate trimethylamine are shown in Figure 5A. With trimethylamine, major differences in the behavior of C30A and wild-type enzymes are seen: the substrate dissociation constant is raised about 100-fold (210 μM and 21.6 mM for wild-type and C30A, respectively), and the limiting rate of flavin reduction is reduced about 30-fold (from 706 to 21.4

Table 3: Reduction Potentials and Atomic Charges for Oxidized Lumiflavin and C6-Methylsulfanyllumiflavin

	planar flavin		butterfly bent flavin	
	lumiflavin	C6-methylsulfanyl-lumiflavin	lumiflavin	C6-methylsulfanyl-lumiflavin
LUMO energy (eV)	+0.665	+0.475	−0.206	−0.321
calcd two-electron reduction potential (mV)	−220	−174[a]	−10	+17
exptl two-electron reduction potential (mV)	−259[b]	−	−	(+40)[c]
charge on C4a (e)[d]	0.153	0.164	0.025	0.033
charge on N5 (e)[d]	−0.682	−0.702	−0.591	−0.597

[a] An experimental value for the reduction potential of 6-*S*-cysteinyl FMN has been measured at −154 mV (*31*), which is close to the value calculated by computational methods for C6-methylsulfanyllumiflavin. [b] Hasford et al. (*9*). [c] Note that this is for C6-cysteinyl FMN incorporated into TMADH; Barber et al. (*32*). [d] Calculated using Mulliken population analysis (*38*).

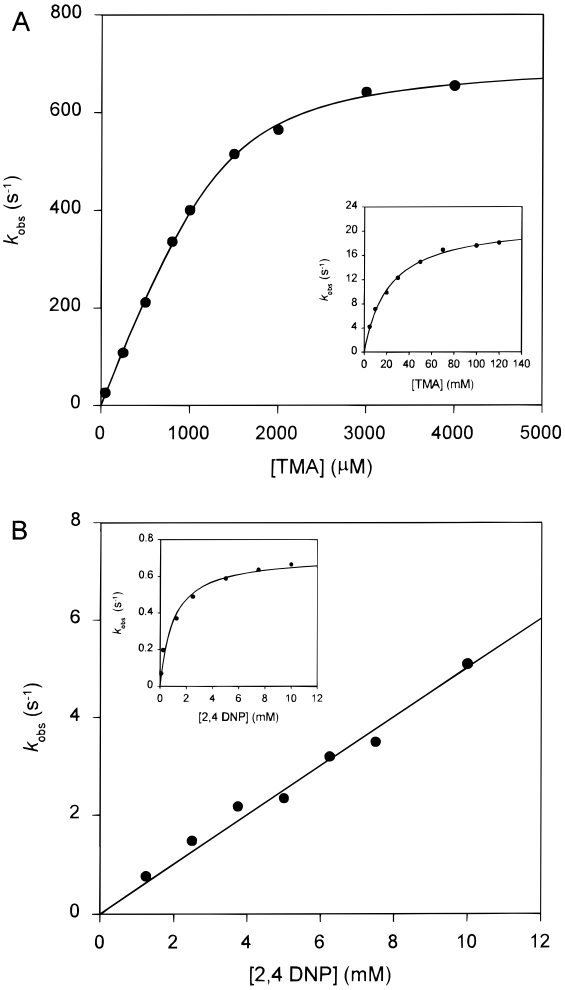

FIGURE 5: Concentration dependence of the observed rate for flavin reduction by trimethylamine and inactivation by 2,4-DNP in wild-type and C30A TMADH. Panel A: plot of k_{obs} as a function of [TMA] for the wild-type protein; $k_{red} = 706 \pm 15$ s^{-1}, $K_d = 210 \pm 60$ μM. Inset: data for the C30A TMADH; $k_{red} = 21.4 \pm 0.4$ s^{-1}, $K_d = 21.6 \pm 1.3$ mM. Reaction conditions: 100 mM potassium phosphate buffer, pH 7.5, 30 °C. Panel B: plot of k_{obs} as a function of [2,4-DNP] for the wild-type protein; second-order rate constant for flavin inactivation, $k = 0.5 \pm 0.01$ mM^{-1} s^{-1}. Inset: data for the C30A TMADH; limiting rate of inactivation, $k_{lim} = 0.74 \pm 0.03$ s^{-1}, $K_d = 1.16 \pm 0.21$ mM. Reaction conditions: 100 mM sodium pyrophosphate buffer, pH 7.7, 30 °C. Enzyme concentration for all experiments was 4 μM.

s^{-1}). Thus, despite the fact that the active sites of wild-type and C30A TMADH are essentially isostructural, the data indicate that catalysis by the C30A enzyme is compromised substantially as a result of mutation.

Kinetic studies involving modification of the 6-*S*-cysteinyl FMN in both wild-type and C30A enzymes with 2,4-dinitrophenylhydrazine provided further evidence for altered reactivity of the 6-*S*-cysteinyl FMN. Wild-type enzyme is readily inactivated by incubation with 2,4-dinitrophenylhydrazine (2,4-DNP) due to the formation of a 6-*S*-cysteinyl FMN C4a phenyl adduct (*28*). Likewise, the C30A protein is also susceptible to inactivation with this reagent (Figure 5B). However, the kinetics of inactivation for the wild-type and C30A enzymes are clearly different: the wild-type exhibits a second-order dependence on [2,4-DNP] (second-order rate constant of 0.5 mM^{-1} s^{-1}), whereas the reaction of the C30A mutant displays saturation kinetic behavior with respect to [2,4-DNP] (with a limiting rate of modification of 0.74 ± 0.03 s^{-1} and an enzyme−2,4-DNP dissociation constant of 1.1 ± 0.2 mM). Thus, the reactivity of the flavin center to inactivation by 2,4-DNP is significantly affected, suggesting electronic differences in the flavin isoalloxazine ring arise as a result of mutation of Cys-30 to Ala.

Computational Studies. The computational studies built on previous attempts to calculate the energies associated with bending of oxidized and reduced flavins [e.g., (*29*, *30*)], and addressed three issues: (i) the role of the butterfly bend in modulating the reduction potential of the flavin, (ii) the reason for the ca. 100-fold increase in K_d for TMA in C30A, and (iii) the reason for the ca. 30-fold decrease in k_{lim} with TMA in C30A. It is apparent from the structure of C30A that the butterfly bend in the flavin does not result from tethering the isoalloxazine ring to the protein via the thioether bond of the 6-*S*-cysteinyl FMN. The reason for this energetically unfavorable nonplanar conformation of the isoalloxazine is as yet unclear, but has been previously debated in terms of modulating the flavin reduction potential [e.g., (*9*)]. Indeed, ab initio calculations on the unrestrained butterfly bent conformation result in a planar conformation. Calculations on both the (energetically favorable) planar and butterfly bent flavin conformations (Table 3) suggest that the butterfly bend raises the two-electron reduction potential from −220 to −10 mV in lumiflavin and from −174 to +17 mV in C6-methylsulfanyllumiflavin. This is in broad agreement with experimental values for the two-electron reduction potential of planar lumiflavin [−259 mV; (*9*)], 6-*S*-cysteinyl FMN [−154 mV; (*31*)], and butterfly bent FMN incorporated into TMADH [+40 mV; (*32*)], and suggests that the formation of the 6-*S*-cysteinyl linkage plays only a minor part in raising the reduction potential. Furthermore, it strongly suggests that the butterfly bend is the major factor in raising the two-electron reduction potential, and that effects of the

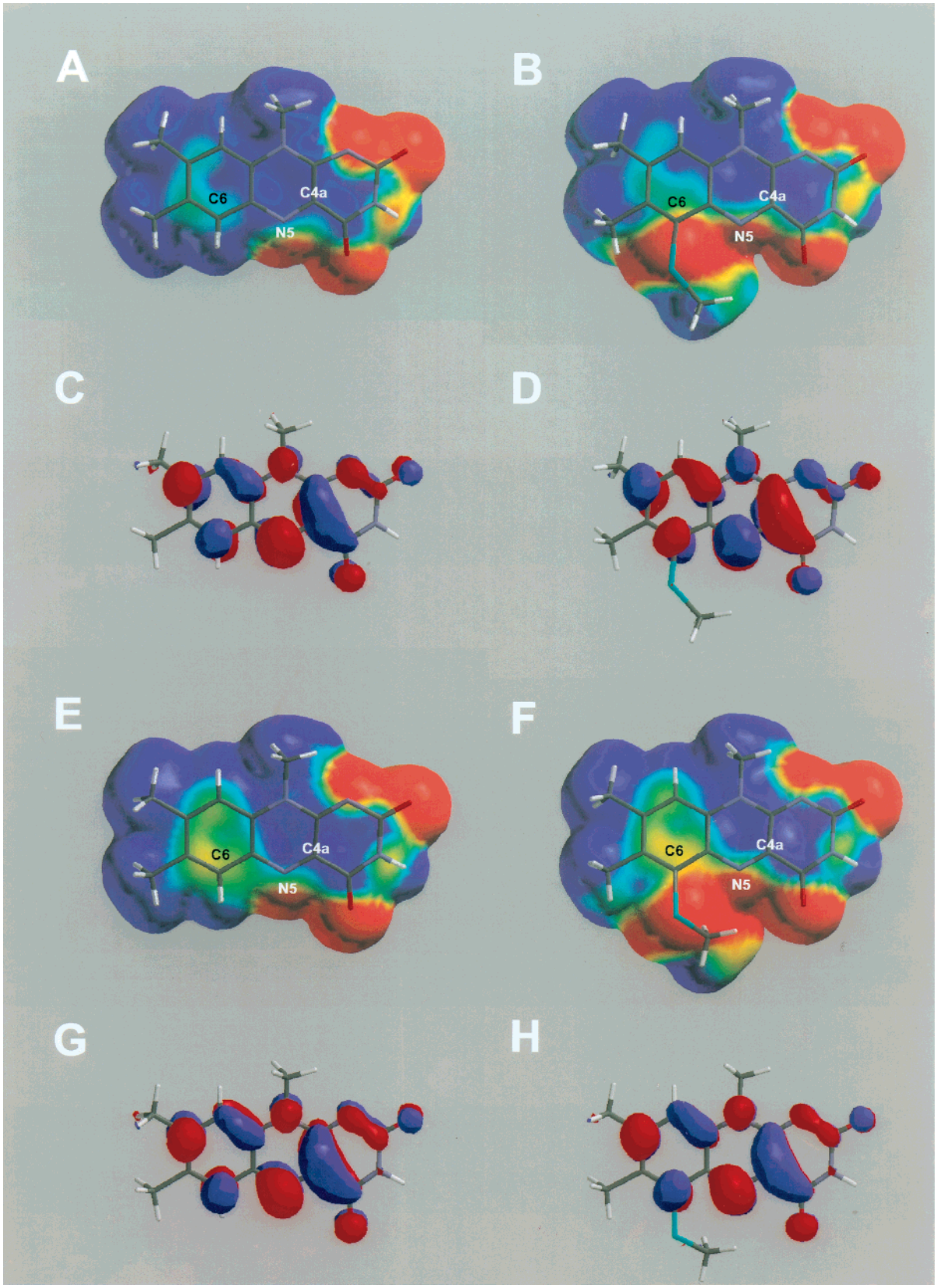

FIGURE 6: Properties of lumiflavin (panels A, C, E, and G) and C6-methylsulfanyllumiflavin (panels B, D, F, and H). Panels A and B: electrostatic potential mapped to the molecular surface of butterfly bent flavins; red corresponds to an electrostatic potential of −10 kcal mol^{-1}, green an electrostatic potential of 0 kcal mol^{-1}, and blue an electrostatic potential of +10 kcal mol^{-1}. Panels C and D: LUMOs of butterfly bent flavins (note that red contours in panel D are equivalent to blue contours in panels C, G, and H, and vice-versa). Panels E and F: electrostatic potential mapped to the molecular surface of planar flavins. Panels G and H: LUMOs of planar flavins. (Note that C6-methylsulfanyllumiflavin and lumiflavin have been used as models of FMN in wild-type and C30A proteins, respectively.)

protein environment (other than to induce the butterfly bend) are relatively minor.

The computational studies also suggest that the observed kinetic differences (a ca. 100-fold increase in K_d and a ca.

30-fold decrease in k_{lim}) arise from a difference between wild-type and C30A proteins in the electrostatic properties of the flavin (Figure 6). These electrostatic differences arise due to the presence or absence of the sulfur in the 6-*S*-cysteinyl linkage to the FMN. In wild-type, with the sulfur atom present, a region of negative charge extends from the C4 carbonyl to the C6 sulfur (Figure 6B), whereas in C30A the corresponding region is significantly smaller, extending from the C4 carbonyl to the flavin N5 (Figure 6A). Electrostatics may play a major role in substrate binding, since substrate is thought to bind as the protonated trimethylammonium cation (*20*, *33*). If this is the case, the computational data suggest that the trimethylammonium cation will bind closer to the C4 carbonyl in the mutant than in the wild type. The precise mechanism of C−H bond cleavage remains to be determined (*20*, *34*). However, the formation of a covalent substrate−flavin adduct has been proposed to follow cleavage of the methyl C−H bond, and the breakdown of this adduct is suggested to gate internal electron transfer from the flavin to the 4Fe-4S center of TMADH (*35*). The identity of the putative adduct is unknown, but the formation of a flavin N5−substrate adduct has been proposed previously (*35*). An alternative is the formation of a flavin C4a−substrate adduct, which is consistent with C4a adduct formation with phenylhydrazine known to occur with TMADH (*28*). Adduct formation could in principle occur (i) after C−H bond breakage (e.g., by homolysis or heterolysis), with the oxidized carbon linking directly into the flavin N5, or (ii) following deprotonation of the substrate nitrogen to release the lone pair for nucleophilic attack at the flavin C4a. This latter adduct would form prior to C−H bond breakage. The mechanism of adduct formation as yet remains elusive as is the mode by which the C−H bond in substrate is broken [for a detailed discussion, see (*20*)]. However, analysis of the LUMOs (Figure 6C,D) suggests that there is significant orbital density on N5 and C4a in both lumiflavin and C6-methylsulfanyllumiflavin consistent with adduct formation at either of these two sites. However, the charge on N5 is much more negative (<-0.5 e) than that on C4a (>0.0 e), implying that C4a may be more likely than N5 for adduct formation. If C4a is the site of adduct formation, this could also help resolve the apparent paradox of why substrate is thought to bind as the protonated trimethylammonium cation [although this aspect remains to be formally demonstrated (*20*)], and yet needs to lose this proton to form the adduct (assuming adduct formation is the result of nucleophilic attack initiated by the lone pair of electrons on the substrate nitrogen atom). The positive electrostatic potential around C4a could reduce significantly the pK_a of substrate, which would then become deprotonated, thus releasing the lone pair for adduct formation. The same argument could apply to N5, but the electrostatic potential at this location is less positive, perhaps making this less likely. Also, the electrostatic potentials (Figure 6E,F), and LUMOs (Figure 6G,H) of planar flavin do not differ greatly from those of the butterfly bent flavin, reinforcing the earlier statement that the principle role of the butterfly bend is modulation of the reduction potential.

Crystallographic studies have established that the nitrogen atoms of the inhibitor tetramethylammonium chloride and the substrate trimethylamine are positioned close to the flavin N5 or C4a in wild-type TMADH (*36*). Given this structural information, it becomes clear how the observed kinetic differences between wild-type and C30A TMADH enzymes might arise. First, since the negative charge on the flavin close to the substrate binding site in C30A is significantly reduced (Figure 6A,B), the electrostatic interaction between the two becomes weaker, thus explaining the ca. 100-fold increase in K_d (in energetic terms $\Delta G_{C30A} - \Delta G_{WT} = \Delta\Delta G_{binding} = -11.5$ kJ mol^{-1}). Second, it is easy to envisage how in wild-type TMADH a positively charged substrate would be located in the middle of the negatively charged patch on the flavin, roughly above either N5 or C4a where it is poised to form either the flavin N5−substrate adduct or the flavin C4a−substrate adduct. However, in the C30A protein, the substrate would bind closer to the C4 carbonyl, and therefore not be optimally positioned to form the covalent adduct, thus providing a rationale for the ca. 30-fold decrease in k_{lim}.

CONCLUSIONS

Recombinant wild-type and C30A TMADH enzymes are essentially isostructural. Thus, the thioether link to the flavin C6 atom in wild-type enzyme is not responsible for the 20° butterfly bending of the flavin. Nevertheless, the butterfly bend is required to raise the reduction potential of the flavin to correspond to the experimentally observed value. Tightly bound inorganic phosphate is present in the deflavo fractions of both recombinant enzymes, preventing reconstitution of each enzyme in vitro by the exogenous addition of FMN. The 6-*S*-cysteinyl link modulates the electrostatic potential around C6 of the flavin isoalloxazine ring in wild-type TMADH. The electronic distribution in wild-type enzyme favors catalysis because the S^{γ} atom of Cys-30 provides an additional electrostatic binding determinant for the protonated substrate molecule and optimally aligns the substrate with either the flavin N5 atom or the flavin C4a atom for electron transfer to the flavin.

NOTE ADDED IN PROOF

The structure of a crystal of thioredoxin reductase from *E. coli* has recently been described (*39*) that has been treated with dithionite to give a reduced active-site disulfide and reduced FAD which exhibits a butterfly bend of the flavin ring of ∼35°. In this case, however, the FAD is non-covalently attached to the protein and the large butterfly bend appears to arise principally from reduction of the flavin ring which is planar in the oxidized enzyme.

REFERENCES

1. Steenkamp, D. J., and Mallinson, J. (1976) *Biochim. Biophys. Acta 429*, 705−719.
2. Lim, L. W., Shamala, N., Mathews, F. S., Steenkamp, D. J., Hamlin, R., and Xuong, N. H. (1986) *J. Biol. Chem. 261*, 15140−15146.
3. Kenney, W. C., McIntire, W., and Steenkamp, D. J. (1978) *FEBS Lett. 85*, 137−140.
4. Steenkamp, D. J., Kenney, W. C., and Singer, T. P. (1978) *J. Biol. Chem. 253*, 2812−2817.
5. Steenkamp, D. J., and Singer, T. P. (1976) *Biochem. Biophys. Res. Commun. 71*, 1289−1295.
6. Ghisla, S., and Massey, V. (1980) *J. Biol. Chem. 255*, 5688−5696.

7. Xia, Z.-X., and Mathews, F. S. (1990) *J. Mol. Biol. 212*, 837−863.
8. Fox, K. M., and Karplus, P. A. (1994) *Structure 2*, 1089−1105.
9. Hasford, J. J., Kemnitzer, W., and Rizzo, C. J. (1997) *J. Org. Chem. 62*, 5244−5245.
10. Boyd, G., Mathews, F. S., Packman, L. C., and Scrutton, N. S. (1992) *FEBS Lett. 308*, 271−276.
11. Barber, M. J., Neam, P. J., Lim, L. W., White, S., and Mathews, F. S. (1992) *J. Biol. Chem. 267*, 6611−6619.
12. Scrutton, N. S., Packman, L. C., Mathews, F. S., Rohlfs, R. J., and Hille, R. (1994) *J. Biol. Chem. 269*, 13942−13950.
13. Huang, L., Scrutton, N. S., and Hille, R. (1996) *J. Biol. Chem. 271*, 13401−13406.
14. Mewies, M., Basran, J., Packman, L. C., Hille, R., and Scrutton, N. S. (1997) *Biochemistry 36*, 7162−7168.
15. Howard, A. J., Nielsen, C., and Xuong, N. H. (1985) *Methods Enzymol. 114*, 452−472.
16. Reeke, G. N. (1984) *J. Appl. Crystallogr. 17*, 125−130.
17. Bethge, P. H. (1984) *J. Appl. Crystallogr. 17*, 215.
18. Brunger, A. T. (1992) in *X-PLOR Version 3.1*, Yale University Press, New Haven, CT.
19. Roussel, A., and Cambillau, C. (1991) in *Silicon Graphics Geometry Partners Directory 86*, Silicon Graphics, Mountain View, CA.
20. Jang, M.-H., Basran, J., Scrutton, N. S., and Hille, R. (1999) *J. Biol. Chem. 274*, 13147−13154.
21. Wilson, E. K., Mathews, F. S., Packman, L. C., and Scrutton, N. S. (1995) *Biochemistry 34*, 2584−2591.
22. Strickland, S., Palmer, G., and Massey, V. (1975) *J. Biol. Chem. 250*, 4048−4052.
23. Basran, J., Mewies, M., Mathews, F. S., and Scrutton, N. S. (1997) *Biochemistry 36*, 1989−1998.
24. Hiromi, K. (1979) *Kinetics of fast enzyme reactions*, Halsted Press, New York.
25. Ridder, L., Zuilhof, H., Vervoort, J., and Rietjens, M. C. M. (1999) in *Flavoprotein Protocols* (Chapman, S. K., and Reid, G. A., Eds.) pp 207−228, Humana Press, Totowa, NJ.
26. Morris, A. L., MacArthur, M. W., Hutchinson, E. G., and Thornton, J. M. (1992) *Proteins: Struct., Funct., Genet. 12*, 345−364.
27. Kasprzak, A. A., Papas, E. J., and Steenkamp, D. J. (1983) *Biochem. J. 211*, 535−541.
28. Nagy, J., Kenney, W. C., and Singer, T. P. (1979) *J. Biol. Chem. 254*, 2684−2688.
29. Zheng, Y.-J., and Ornstein, R. L. (1996) *J. Am. Chem. Soc. 118*, 9402−9408.
30. Dixon, D. A., Lindner, D. L., Branchaud, B., and Lipscomb, W. N. (1979) *Biochemistry 18*, 5770−5775.
31. Ghisla, S., Kenney, W. C., Knappe, W. R., McIntire, W., and Singer, T. P (1980) *Biochemistry 19*, 2537−2544.
32. Barber, M. J., Pollock, V., and Spence, J. T. (1988) *Biochem. J. 256*, 657−659.
33. Raine, A. R., Yang, C. C., Packman, L. C., White, S. A., Mathews, F. S., and Scrutton, N. S. (1995) *Protein Sci. 4*, 2625−2628.
34. Basran, J., Sutcliffe, M. J., Hille, R., and Scrutton, N. S. (1999) *Biochem. J. 341*, 307−314.
35. Rohlfs, R. J., and Hille, R. (1994) *J. Biol. Chem. 269*, 30869−30879.
36. Bellamy, H. D., Lim, L. W., Mathews, F. S., and Dunham, W. R. (1989) *J. Biol. Chem. 264*, 11887−11992.
37. Kleywegt, G. J., and Brünger, A. T. (1996) *Structure 4*, 897−904.
38. Mulliken, R. S. (1955) *J. Chem. Phys. 23*, 1833−1840.
39. Lennon, B. W., Williams, C. H., Jr., and Ludwig, M. L. (1999) *Protein Science 8*, 2366−2379.
40. Carson, M. (1997) *Methods Enzymol. 277*, 493−505.

BI9927181